# Magnetism and superconductivity in $Y_{1-x}Tb_xNi_2B_2C$ single crystals

B. K. Cho,[1] H. B. Kim,[1] and Sung-Ik Lee[2]
[1]*Center for Frontier Materials, Department of Materials Science and Engineering, Kwangju Institute of Science and Technology, Kwangju, 500-712, Korea*
[2]*National Creative Research Initiative Center for Superconductivity and Department of Physics, Pohang University of Science and Technology, Pohang, 790-784, Korea*
(Received 19 January 2000; revised manuscript received 9 October 2000; published 23 March 2001)

The magnetic and superconducting properties in a series of pseudo-quaternary compounds $Y_{1-x}Tb_xNi_2B_2C$ were investigated by the temperature-dependent magnetization $M(T)$ for applied field parallel and perpendicular to the $c$ axis and by in-plane resistivity, $\rho(T)$. There was a large anisotropy in $M(T)$, which is attributed to the crystalline electric field effects. As the Tb concentration $x$ is increased, the superconducting transition temperature $T_c$ decreases and disappears rapidly in the vicinity of $x=0.4$ while the Néel temperature $T_N$ appears abruptly near $x=0.4$ and increases with Tb content. In addition, the increase of $M(T)$ at low temperatures below $T_N$ was observed for $x \geqslant 0.4$, of which the onset temperature $T_{WF}$ is regarded as development of weak-ferromagnetic component. $T_{WF}$ was also in proportion to the Tb content $x$ accompanied by $T_N$. The linear decrease of $T_c$ for dilute Tb concentration seems to follow an Abrikosov-Gor'kov expectation, while the sudden destruction of $T_c$ near $x=0.4$ seems to have close correlation with the emergence of magnetic states, i.e., antiferromagnetic and weak-ferromagnetic states. Possible scenarios for the correlation are discussed.

DOI: 10.1103/PhysRevB.63.144528 PACS number(s): 74.70.Dd, 74.62.−c, 74.25.Ha

## I. INTRODUCTION

The quaternary borocarbides $RNi_2B_2C$ ($R=$Y), rare-earth elements have been continuously studied after discovery of the compounds in 1994 because of not only their comparatively high superconducting transition temperatures up to $T_c \approx 16$ K with $R=$Lu but also the coexistence of superconductivity and magnetism.[1–3] Even though they have a layered-tetragonal structure alternating $R$C sheets and $Ni_2B_2$ layers,[4] which is reminiscent of high $T_c$ cuprate superconductors, electronic band structure calculations demonstrated that they are electronically three dimensional. It was also shown that Ni $3d$ electrons predominantly contribute to the conduction band at the Fermi level, although the electronic contributions from the other elements B and C are not negligible.[5,6]

Among the $RNi_2B_2C$ family, $TbNi_2B_2C$ is not superconducting above 300 mK but undergoes an antiferromagnetic ordering at $T_N=15$ K with Tb moments lying in [001] direction.[7] $TbNi_2B_2C$ exhibited an additional magnetic transition below 8 K in antiferromagnetically ordered state, which was identified as weak-ferromagnetic transition by magnetization, resistivity, and specific-heat measurements.[7,8] Neutron-diffraction measurements also suggested the presence of a small-ferromagnetic component.[9] The origin of nonsuperconductivity in $TbNi_2B_2C$ is still under debate. One of the possibilities is a noncollinear antiferromagnetic spin structure of Tb moments. In fact, the magnetic hyperfine field at the Ni site, which could act as the pair-breaking field at Ni site, was observed in the Mössbauer spectroscopy.[10] The study of pseudoquaternary compound, $Er_{1-x}Tb_xNi_2B_2C$ was reported. It was conjectured that the weak-ferromagnetic component does not directly affect the superconductivity. However, it should be noted that there are complications in ground-magnetic structure in above compounds because the magnetic structure in $ErNi_2B_2C$ is quite different from the one in $TbNi_2B_2C$.[11]

Based on the Abrikosov-Gor'kov (AG) theory in the dilute magnetic impurity limit, $T_c$ decreases linearly with the de Gennes factor, $(g_J-1)^2J(J+1)$, where $g_J$ is the Landé $g$ factor and $J$ is the total angular momentum of the magnetic-impurity element. The de Gennes factor indicates the strength of the exchange coupling between the local moments and the conduction electrons. For pure-quaternary compounds, $T_c$ seems to scale well with the de Gennes factor of the rare earth.[12] However, complete breakdown of de Gennes scaling was reported in pseudoquaternary system, $Ho_{1-x}Dy_xNi_2B_2C$ and $Lu_{1-x}Dy_xNi_2B_2C$.[13] Because Dy spins in $DyNi_2B_2C$, which is in the next site of Ho in the Periodic Table, have almost the same antiferromagnetic structure as the Ho spins in $HoNi_2B_2C$,[14–16] almost no change in magnetic structure of $Ho_{1-x}Dy_xNi_2B_2C$ below $T_N$ will be introduced by alloying of Ho and Dy. It was noticed that the effective magnetic field at the Ni site will be cancelled out in antiferromagnetically ordered state by consideration of crystal symmetry and magnetic structure in $Ho_{1-x}Dy_xNi_2B_2C$ system so that the superconductivity can survive under the antiferromagnetically ordered ground state in $DyNi_2B_2C$.[17] On the other hand, for $Lu_{1-x}Dy_xNi_2B_2C$, $Lu^{3+}$ ion seems to act as nonmagnetic impurity in Dy-rich compound and thus bring about a pair-breaking effect.[13,17]

It will be of great interest to investigate the superconducting, magnetic properties and their interplay in $Y_{1-x}Tb_xNi_2B_2C$ compounds. Because the host compound, $YNi_2B_2C$, is nonmagnetic, there will be no complication of ground state magnetic structure, such as $Er_{1-x}Tb_xNi_2B_2C$. In this paper, we report magnetic and superconducting measurements of $Y_{1-x}Tb_xNi_2B_2C$ single crystals and a systematic study of the pair-breaking effects in this system.

 ©2001 The American Physical Society

## II. EXPERIMENTS

Sizable single crystals of $Y_{1-x}Tb_xNi_2B_2C$ ($x=0.05$, 0.1, 0.15, 0.2, 0.25, 0.3, 0.4, 0.5, 0.6, and 0.8) were grown by flux method using $Ni_2B$ as a solvent, as described in detail elsewhere.[18] Stoichiometric $Y_{1-x}Tb_xNi_2B_2C$ mixtures of high-purity Y (99.99%), Tb (99.99%), Ni (99.95%), B (99.7%), C (99.99 %) were all arc-melted under a flowing Ar gas atmosphere and the melted button was flipped over several times to have homogeneous mixture. Estimated mass loss during the first arc-melting was less than 1 wt %. The arc-melted polycrystalline $Y_{1-x}Tb_xNi_2B_2C$ button was placed on top of $Ni_2B$ fragments in an alumina crucible with the mass ratio of approximately 1:1.5, respectively. The sample assembly was located in the middle of a vertical tube furnace, in which Ar gas was flowing to make oxygen free. The samples are heated up to 1500 °C and cooled slowly in the similar thermal cycle reported elsewhere.[18] After completion of the thermal treatment, $Ni_2B$ was solidified in the crucible through congruent melting, with the single crystals being inside the flux. The crucible was placed in a vacuum-sealed quartz ampoule and then the ampoule was heated to 1200 °C and stayed for about an hour to make $Ni_2B$ melt sufficiently. The ampoule was taken out of the furnace, inverted and quickly spun in the centrifuge. Then, the crystals were extracted from the liquid flux by mechanical force. All of the peaks of x-ray diffraction pattern for the pulverized-single crystals were well indexed in terms of tetragonal lattice structure with $I4/mmm$ symmetry group, indicating that they are of single phases without any noticeable impurity peak, which was found in the initial polycrystalline sample. It was shown that the grown crystals are platelike and the $c$ axis of the single crystals is normal to their flat surface.

dc magnetization measurements were performed with a superconducting quantum interference device (SQUID) magnetometer (quantum design MPMS). The zero-field electrical resistivity was measured by standard four-probe method under the temperature and field control of the SQUID, using Keithley dc current source and Hewlett Packard nanovoltmeter.

## III. RESULTS

Figure 1 shows the temperature-dependent magnetization of $Y_{1-x}Tb_xNi_2B_2C$ compounds in an applied field, $H=10$ kG, parallel ($\mathbf{H}\|\mathbf{c}$) and perpendicular ($\mathbf{H}\perp\mathbf{c}$) to the $c$ axis for $x=0.1$ and 0.6. Similarly for all $x$ values, including $x=0.1$ and 0.6, the anisotropy between ($\mathbf{H}\|\mathbf{c}$) and ($\mathbf{H}\perp\mathbf{c}$) becomes pronounced as the temperature goes down. The magnetization for ($\mathbf{H}\perp\mathbf{c}$) is much larger than for ($\mathbf{H}\|\mathbf{c}$) as in $TbNi_2B_2C$, indicating that Tb spins lie predominantly in the plane normal to $c$ axis. This anisotropy is attributed to the crystalline electric field (CEF) effect, which is the electrostatic effect due to the surrounding charges.[19] Although both curves at high temperatures follow the Curie-Weiss law, $M/H=C/(T-\theta)$ where $\theta$ is the Weiss temperature, and Curie constant, $C=N\mu_{eff}^2/3k_B$ with $N$ of the number of Tb ion per mole formula unit, significant deviations are observed at low temperatures. For $x\leqslant 0.3$, a slight deviation of $M/H$ from the Curie-Weiss law, which is shown in the inset of Fig. 1(a) near $T=9$ K, is attributed to its superconducting diamagnetism. However, for $x\geqslant 0.4$, the magnetization shows saturation behavior at low temperatures due to the antiferromagnetic (AF) ordering of the Tb moments, as in Fig. 1(b).

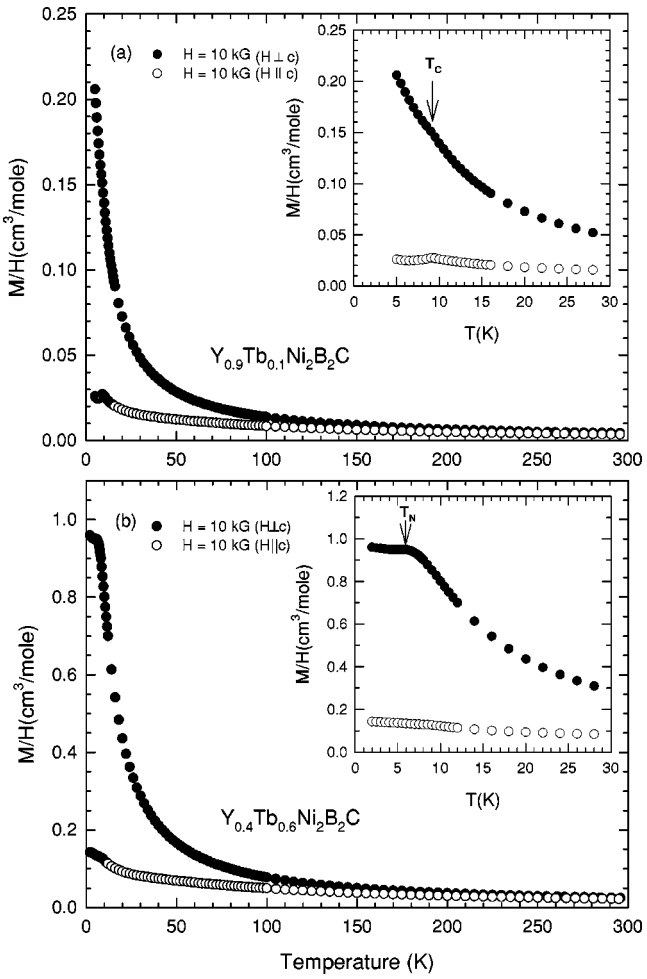


FIG. 1. Magnetization as a function of temperature for single crystals in an applied-magnetic field $H=10$ kG for $\mathbf{H}\perp\mathbf{c}$ (filled circles) and for $\mathbf{H}\|\mathbf{c}$ (open circles) for (a) $Y_{0.9}Tb_{0.1}Ni_2B_2C$, (b) $Y_{0.4}Tb_{0.6}Ni_2B_2C$. Inset: Expended plot in low-temperature region.

The inverse-magnetic susceptibility $\chi^{-1}\equiv(M/H)^{-1}$, which is plotted in Fig. 2, is linear at high temperatures but deviates from the linear Curie-Weiss behavior at low temperatures. We have found two parameters $\mu_{eff}$ and $\theta$ by fitting the susceptibility data to the Curie-Weiss law in high temperature region above 100 K for each $x$, as shown by the fitting lines in Fig. 2. The values of $\mu_{eff}$ for both field orientations, which are listed in Table I, are within $\approx 5\%$ of the theoretical effective magnetic moment, $\mu_{eff}=9.72\mu_B$ for an isolated $Tb^{3+}$ ion, except for $x=0.3$. The difference of the $\theta$ values between the field orientations is mainly again due to the CEF effects. According to the point charge model of CEF, the sign of $(\theta_\perp-\theta_\|)$ is a decisive factor in determining the easy axis. Thus, the positive values of $(\theta_\perp-\theta_\|)$ for all $x$ indicate the easy magnetic plane normal to the $c$ axis in $Y_{1-x}Tb_xNi_2B_2C$.

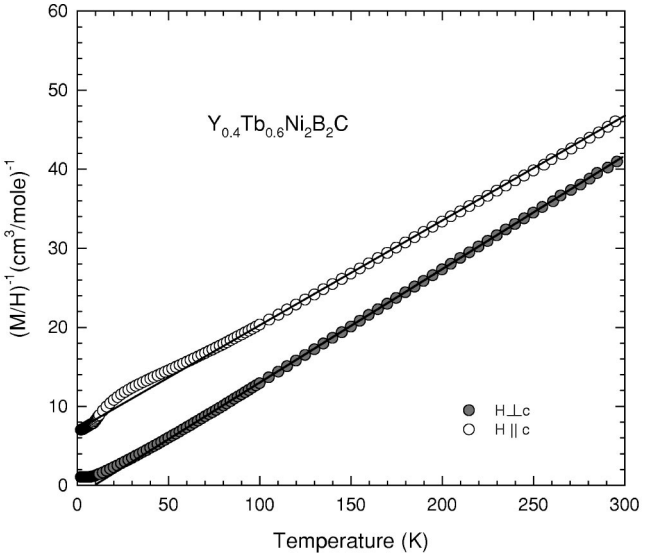


FIG. 2. Inverse magnetization as a function of temperature for a single crystal of $Y_{0.4}Tb_{0.6}Ni_2B_2C$ from the data in Fig. 1(b) for $\mathbf{H}\perp\mathbf{c}$ (filled circles) and for $\mathbf{H}\|\mathbf{c}$ (open circles).

Large anisotropy was also observed in the field-dependent magnetization, $M(H)$, for the applied fields of $0\leqslant H\leqslant 50$ kG for $\mathbf{H}\|\mathbf{c}$ and $\mathbf{H}\perp\mathbf{c}$. A magnetic field induced phase transition at $T=2$ K for $\mathbf{H}\perp\mathbf{c}$ near $H=18$ kG, which appears broadly for small concentration of Tb, became more pronounced at $x=0.8$, as seen in Fig. 3(a). This manifests field-induced ferromagnetic transitions from AF state. Moreover, the $M(H)$ curve for $x=0.8$ shows nonlinear behavior at 2 K and in the low-field region as shown in the inset of Fig. 3(a). Considering the weak-ferromagnetic state in $TbNi_2B_2C$, this nonlinearity of $M(H)$ can be attributed to the development of weak-ferromagnetic component. The extrapolation of the linear magnetization for 5 kG$\leqslant H\leqslant$10 kG to the zero field gives a spontaneous ferromagnetic component of $\approx 0.16\mu_B$, much smaller than the value of $\approx 0.5\mu_B$ in $TbNi_2B_2C$. The magnetization for $\mathbf{H}\perp\mathbf{c}$ at low temperatures is saturated at high fields. The saturated moments at $T=2$ K were $8.27\mu_B$, $7.64\mu_B$, $8.13\mu_B$, $10.69\mu_B$,

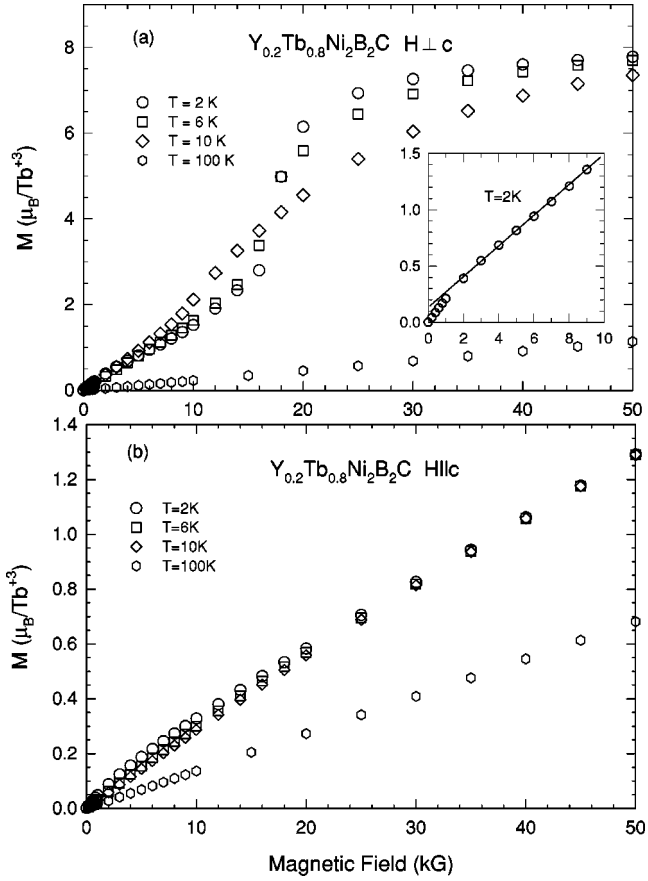


FIG. 3. Magnetization ($M$) as a function of applied magnetic field for a single crystal of $Y_{0.2}Tb_{0.8}Ni_2B_2C$ at several temperatures: (a) $\mathbf{H}\perp\mathbf{c}$, (b) $\mathbf{H}\|\mathbf{c}$. Inset: Expended plot in low-field region. Note the different $M$ scale for (a) and (b).

$6.76\mu_B$, $7.72\mu_B$, $7.99\mu_B$, and $7.78\mu_B$ for $x=0.15$, 0.2, 0.25, 0.3, 0.4, 0.5, 0.6, and 0.8, respectively, which are significantly smaller than the theoretical value of $9\mu_B$ for an isolated $Tb^{3+}$ ion except for $x=0.3$. There may be another field-induced magnetic transition at higher fields than 50 kG. The high-field transitions were observed in $HoNi_2B_2C$ and the transition fields depended upon the field angle within the

TABLE I. Weiss temperatures ($\theta$) and effective-magnetic moments ($\mu_{eff}$) for magnetic fields parallel and perpendicular to the $c$ axis in crystals of $Y_{1-x}Tb_xNi_2B_2C$. The values are obtained by fitting the data for each sample to the Curie-Weiss equation, $M/H=C/(T-\theta)$ and $C=N\mu_{eff}^2/3k_B$ (see text).

| $x$ | $\theta$ (K) ($\mathbf{H}\perp\mathbf{c}$) | $\theta$ (K) ($\mathbf{H}\|\mathbf{c}$) | $\mu_{eff}(\mu_B/\mathrm{Tb})(\mathbf{H}\perp\mathbf{c})$ | $\mu_{eff}(\mu_B/\mathrm{Tb})(\mathbf{H}\|\mathbf{c})$ |
|---|---|---|---|---|
| 0.05 | $-10.66\pm0.91$ | $-80.45\pm0.54$ | $9.60\pm0.60$ | $10.20\pm0.40$ |
| 0.1 | $14.71\pm1.06$ | $-45.19\pm0.45$ | $9.80\pm0.80$ | $9.90\pm0.40$ |
| 0.15 | $9.90\pm0.49$ | $-59.74\pm0.15$ | $9.93\pm0.53$ | $10.2\pm0.27$ |
| 0.2 | $2.46\pm0.26$ | $-54.66\pm0.28$ | $9.75\pm0.35$ | $9.7\pm0.35$ |
| 0.25 | $7.80\pm0.12$ | $-49.41\pm0.25$ | $9.60\pm0.24$ | $10.08\pm0.32$ |
| 0.3 | $2.60\pm0.34$ | $-50.97\pm0.42$ | $12.00\pm0.47$ | $11.80\pm0.50$ |
| 0.4 | $5.71\pm0.74$ | $-42.50\pm0.60$ | $10.18\pm0.55$ | $9.75\pm0.60$ |
| 0.5 | $10.40\pm0.18$ | $-52.44\pm0.47$ | $9.78\pm0.28$ | $10.16\pm0.42$ |
| 0.6 | $8.79\pm0.32$ | $-54.00\pm0.55$ | $9.65\pm0.37$ | $10.07\pm0.45$ |
| 1.0 | $16.00\pm1.00$ | $-60.00\pm1.00$ | $9.70\pm0.10$ | $9.90\pm0.10$ |

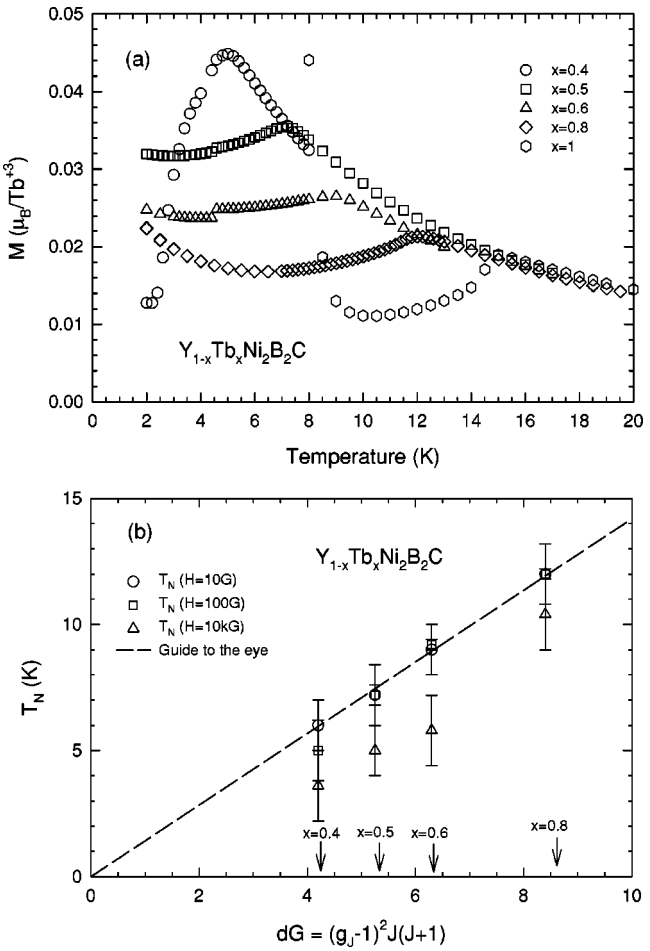


FIG. 4. (a) Normal-state magnetization as a function of temperature in applied field $H=100$ G (**H**$\|$**c**) for single crystals of $Y_{1-x}Tb_xNi_2B_2C$. (b) Neel temperature $T_N$ versus de Gennes factor, $D=(g_J-1)^2J(J+1)$, determined from the data in (a).

plane normal to $c$ axis.[20] The large value of saturated magnetization for $x=0.3$, together with the large $\mu_{eff}$ in Table I, is still in question and under study. A simple possible explanation is that the $Tb^{3+}$ ion in $x=0.3$ compound, somehow, is influenced by polarization of the conduction electron spins due to the exchange interaction between the local moments and the conduction electrons. The question is why the polarization is unique in $x=0.3$? Contrary to Fig. 3(a) for **H**$\perp$**c**, M(H) in Fig. 3(b) for **H**$\|$**c** shows an ordinary paramagnetic behavior. It seems that applied fields along a hard axis seldom have an influence on magnetic ordering of Tb ions.

In order to identify the magnetic ordering transitions, we have measured the temperature-dependent magnetization, $M(T)$, for $H=100$ G (**H**$\perp$**c**). The AF-ordering temperature $T_N$ defined by the maximum slope of the magnetization curve near the transition, can be seen from $x=0.4$ and is obviously increased with Tb doping, as shown in Fig. 4(a). Moreover, $T_N$ has linear dependence on the de Gennes factor, which is consistent with the Ruderman-Kittel-Kasuya-Yosida (RKKY) indirect exchange model for AF transition. The de Gennes factor for the compounds studied in this paper is weighted by Tb concentration. The $T_N$ is suppressed gradually as the external field is increased up to 10 kG, as

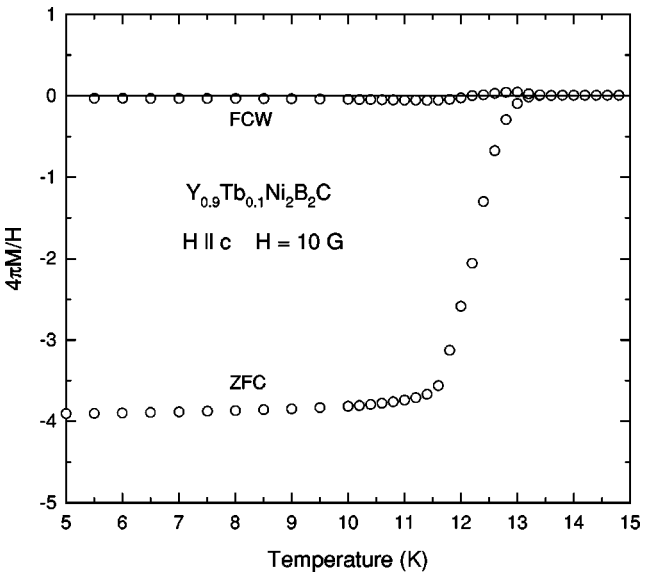


FIG. 5. Superconducting volume magnetization as a function of temperature for a single crystal of $Y_{0.9}Tb_{0.1}Ni_2B_2C$ in an applied-magnetic field, $H=10$ G (**H**$\|$**c**). Both field-cooled (FC) and zero-field-cooled (ZFC) data are shown.

plotted in Fig. 4(b). For $x=0.4$, $T_N$ and $T_c$ are so close that it is difficult to distinguish them in magnetization data near $T=5.5$ K.

In addition, anomalous increasing behavior in $M(T)$ at low temperatures below $T_N$ is observed for $x\geqslant 0.4$ as seen in Fig. 4(a) and enhanced with increasing Tb concentration. Together with the data of $TbNi_2B_2C$ in Refs. 8–10 and weak-ferromagnetic component found in $M(H)$ curve in Fig. 3, the onset of the increase in $M(T)$ at lower temperatures is regarded as indication of development of weak-ferromagnetic component, defined as $T_{WF}$.

To investigate the superconductivity of these materials, low field magnetization measurement was performed on each sample for **H**$\|$**c**, where the superconductivity is well observed with minimum obstruction by the magnetic contributions of $Tb^{3+}$ ions. In Fig. 5, for the case of $x=0.1$, zero-field-cooled (ZFC) magnetization data, remarkably lower than field-cooled (FC) data, shows distinct diamagnetic magnetization at temperatures below 13.4 K. $T_c$ was determined by the onset of the diamagnetic drop of ZFC magnetization. In FC magnetization data, a small bump around $T_c$ in Fig. 5 is observed, which seems to arise from spin alignment by the external field penetrating into the imperfect superconductor during the superconducting transition. Moreover, an anomalous paramagnetic Meissner state was occasionally detected in FC magnetization measurement for some cases of $x$, which can be attributed to significant field inhomogeneity at low-magnetic field in our measurement system. In ZFC magnetization data of Fig. 5, the volume fraction for magnetic shielding is more than 100% due to the demagnetization effect, which is not corrected in this paper.

The relative in-plane electrical resistivity as a function of temperature in the zero-applied field is plotted in Fig. 6. It shows that a sharp superconducting transition above $T=2$ K exists up to $x=0.4$ and vanishes for $x\geqslant 0.5$. The $T_c$

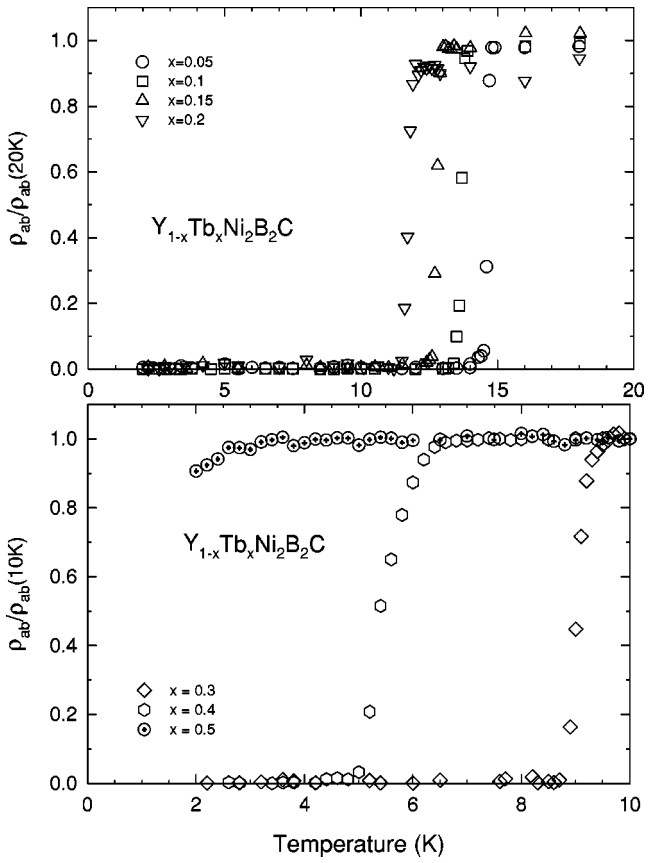


FIG. 6. Normalized in-plane electrical resistivity as a function of temperature in zero-applied magnetic field for single crystals of $Y_{1-x}Tb_xNi_2B_2C$.

was determined by an intersection of the maximum slope of the transition with normal-state resistivity near the sudden drop. The $T_c$ rapidly decreases with increasing Tb content, which is similar to the results from the low-field magnetization data. In high-temperature range, normal-state resistivity shows linear temperature dependence as that of typical metal. High residual resistivity ratios, $\rho(300\ \mathrm{K})/\rho(T)$, in Table II, indicate that this sample is of good quality, as in $TbNi_2B_2C$ of $\rho(400\ \mathrm{K})/\rho\ (2\mathrm{K}) = 19$. We could not clearly distinguish any resistance loss in terms of magnetic scattering near AF transition.

The transition temperatures, $T_c$, $T_N$, and $T_{WF}$ as a function of the de Gennes factor are all together exhibited in Fig.

TABLE II. Residual resistivity ratio for crystals of $Y_{1-x}Tb_xNi_2B_2C$. The resistivity measurement is carried out in zero-applied magnetic field in plane normal to *c* axis.

| $x$ | Residual resistivity ratio |
|---|---|
| 0.05 | $\rho_{ab}(300\ \mathrm{K})/\rho_{ab}(16\ \mathrm{K}) = 11.6$ |
| 0.1 | $\rho_{ab}(300\ \mathrm{K})/\rho_{ab}(14\ \mathrm{K}) = 9.15$ |
| 0.15 | $\rho_{ab}(300\ \mathrm{K})/\rho_{ab}(13.5\ \mathrm{K}) = 8.94$ |
| 0.2 | $\rho_{ab}(300\ \mathrm{K})/\rho_{ab}(13\ \mathrm{K}) = 8.94$ |
| 0.25 | $\rho_{ab}(300\ \mathrm{K})/\rho_{ab}(12\ \mathrm{K}) = 6.64$ |
| 0.3 | $\rho_{ab}(300\ \mathrm{K})/\rho_{ab}(12\ \mathrm{K}) = 7.8$ |

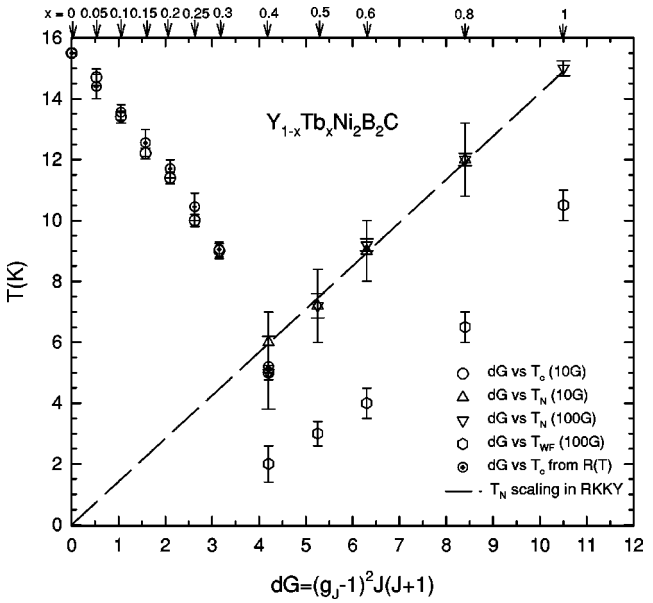


FIG. 7. Transition temperatures, $T_c$, $T_N$, and $T_{WF}$, as a function of de Gennes factor, $D=(g_J-1)^2J(J+1)$, from magnetization and resistivity measurements for single crystals of $Y_{1-x}Tb_xNi_2B_2C$.

7. The de Gennes factor for the $Y_{1-x}Tb_xNi_2B_2C$ compounds is scaled with Tb concentration. As Tb concentration $x$ is increased, $T_c$ is reduced and disappears near $x=0.4$, while $T_N$ is linearly increased above $x=0.4$ and $T_{WF}$ is gradually enhanced above $x=0.4$ at lower temperatures. This diagram is quite different from the polycrystalline data of Bitterlich *et al.*[21] The transition temperatures of polycrystals in Ref. 21 are a little bit lower and less clear than those of single crystals in this paper. While the $T_c$ variation shows similar behavior for both cases, significant difference between the two cases is found in the magnetic transition temperatures. The $T_N$ and $T_{WF}$ in this work are found for wider range of Tb concentration than those in Ref. 21, resulting in the narrow range of overlapping of magnetism and superconductivity at $x=0.4$.

## IV. DISCUSSION

It was shown that the large anisotropy in $RNi_2B_2C$ compounds mainly is due to the CEF splitting of the ground multiplets of $R$ ion.[19] In the $RNi_2B_2C$ compounds, the crystal-field Hamiltonian can be expressed as

$$H_{CEF}=B_2^0O_2^0+B_4^0O_4^0+B_4^4O_4^4+B_6^0O_6^0+B_6^4O_6^4, \qquad (1)$$

where the $B_n^m$ are CEF parameters to be determined experimentally and the $O_n^m$ are Stevens equivalent operators. Among the CEF parameters, the first term $B_2^0$ is dominant and the initial estimation of the value of $B_2^0$ is important in analyzing the anisotropic $M(T)$ in a CEF scheme. Wang and Boutron showed that only the $B_2^0$ term among the terms in the CEF Hamiltonian contributes to the high-$T$ Weiss temperatures in single crystals with $R$.[22]

From the expansion of the susceptibility as a power series in $1/T$, the value of $B_2^0$ can be calculated from the difference between $\theta_\parallel$ and $\theta_\perp$ using the relation

$$B_2^0 = \frac{10}{3(2J-1)(2J+3)}(\theta_\perp - \theta_\parallel), \tag{2}$$

where $J$ is the total angular momentum of the isolated ion. The above equation is derived based on the assumption of uncoupled ions, i.e., no exchange interaction between rare-earth ions. In addition, it was shown that the anisotropic exchange interaction between $Ho^{3+}$ ions in $HoNi_2B_2C$ is in part responsible to the observed magnetic anisotropy.[19] It is plausible for us to use the value of $(\theta_\perp - \theta_\parallel)$ for dilute Tb concentration compounds to evaluate the $B_2^0$ value because the exchange interaction is expected to be negligible in $Y_{1-x}Tb_xNi_2B_2C$ $(x \ll 1)$ compared to that in $Y_{1-x}Tb_xNi_2B_2C$ $(x \approx 1)$ due to the dilute concentration of $Tb^{3+}$ ions in the former compounds, whereas the CEF effects should be nearly same in the two crystals. By using the Weiss-temperature in $Y_{1-x}Tb_xNi_2B_2C$ $(x=0.05,0.1)$, $B_2^0$ is found to be 1.43 K and 1.21 K, which is smaller than the $B_2^0 = 1.54$ K for $TbNi_2B_2C$. Therefore, it can be conjectured that the anisotropic interatomic exchange interaction acts to cause larger difference of Weiss-temperatures between $\mathbf{H} \| \mathbf{c}$ and $\mathbf{H} \perp \mathbf{c}$.

The superconducting and magnetic transition temperatures are together plotted versus effective de Gennes factor of $Y_{1-x}Tb_xNi_2B_2C$ in Fig. 7. As can be seen, the strong correlation exists between each transition temperature and Y/Tb concentration ratio and between superconducting transition and two magnetic transitions. For low concentration of $Tb^{3+}$ $(x \leqslant 0.25)$, linear dependence of $T_c$ in terms of de Gennes value is observed as can be expected by Abrikosov-Gor'Kov (AG) theory that describes the magnetic impurity effect on the superconductivity in terms of the exchange interaction between localized magnetic electrons and conduction electrons forming superconducting pair below $T_c$. The initial reduction of $T_c$ due to magnetic pair breaking is given as

$$\frac{T_c}{T_{c0}} = 1 - \frac{c}{2}\frac{N(0)I^2}{8k_B T_{c0}}\psi'\left(\frac{1}{2}\right)D, \tag{3}$$

where $c$ is the concentration of the magnetic impurity, $\psi'(\frac{1}{2}) = 4.96$ is a derivative of digamma function evaluated at $\frac{1}{2}$, $N(0)$ is the density of states at the Fermi level and $I$ is the exchange constant between the local and conduction electron spins. The $N(0)$ of the $RNi_2B_2C$ compounds should be very similar to the $N(0)$ of $LuNi_2B_2C$, differing only by the filling of the $4f$ levels which was shown not to contribute to the conduction band.[5,6] The density of states at the Fermi level can be estimated to be 7/eV per formula unit from the measured $\gamma \approx 19$ mJ/mol $K^2$ for $YNi_2B_2C$ and for $LuNi_2B_2C$ that is larger than the value of $\approx 4.8$/eV per formula unit from electronic band calculation. Using the approximate initial slope of reduction of $T_c$ with de Gennes factor in Fig. 7 for $Y_{1-x}Tb_xNi_2B_2C$, the exchange constant is found to be $I \approx 11.5$ meV.

The de Gennes scaling of all $T_c$, $T_N$, and $T_{WF}$ indicate that the electronic and magnetic properties in $Y_{1-x}Tb_xNi_2B_2C$ compound are closely correlated by the same origin of the exchange interactions between localized magnetic moments and itinerant conduction electrons. Of great interest is the behavior of each transition at $x=0.4$ in $Y_{1-x}Tb_xNi_2B_2C$. Sudden disappearance of superconductivity above $x>0.4$ seems to have close correlation with appearance of both AF ordering and weak-ferromagnetic component. For the single crystal of $Y_{0.6}Tb_{0.4}Ni_2B_2C$, all of three ground states, superconductivity, AF state, and weak ferromagnetic component are observed simultaneously as temperature is lowering below $T_c$. Because of the coexistence of the three ground states, the sudden suppression of superconductivity near $x=0.4$ seems to be closely related with appearance of magnetic state.

Contrary to AG scheme for the dilute $Tb^{3+}$ concentration, it is unlikely that the exchange pair breaking effect can be considered as a main contribution to pair breaker, i.e., Tb concentration of $x=0.4$ is enough to give de Gennes factor above the critical value in AG universal curve. Recently critical de Gennes value of $Er_{1-x}Tb_xNi_2B_2C$ compounds is estimated to be around 5.2, which is larger than the de Gennes factor for $Y_{0.6}Tb_{0.4}Ni_2B_2C$. However, the estimation was made under the assumption of different exchange integral depending upon the rare-earth element. Our estimation of exchange integral of 11.5 meV, which is 0.75 eV Å$^3$, is smaller than the one from the Ref. 23, $I=0.89$ eV Å$^3$, so that the critical de Gennes factor even should be larger than their estimation. It was also shown that the confinement of magnetic moment in the plane perpendicular to the $c$ axis due to CEF effect, which is shown in Figs. 1 and 2, makes the exchange interaction less effective as a pair breaker.

Another explanation of disappearance of superconductivity is related with the emergence of AF ordering. The phenomenological theory is recently developed to explain the $T_c$ variation in terms of de Gennes factor in $Ho_{1-x}Dy_xNi_2B_2C$, utilizing the magnetic structure in AF state.[17] In the case of pure $TbNi_2B_2C$, below $T_N$, three of the Tb moments that are the nearest neighbors of Ni atom align in the [100] direction and one of them is in opposite orientation. A net magnetic field at the Ni site, which is located at the center of tetrahedron, composed of the nearest rare-earth ions and mainly contributes to the superconductivity, is not completely cancelled by the AF ordering. There is a possibility that the pair-breaking below $T_N$ is brought about by the remnant field at the Ni site. Hence, this model can explain the sudden quench of superconductivity near $x=0.4$ in $Y_{1-x}Tb_xNi_2B_2C$. In addition to the AF ordering, the weak ferromagnetic component also appears at the same composition. Although the weak ferromagnetic component seems not to directly affect the pair breaking in $Er_{1-x}Tb_xNi_2B_2C$,[23] it should not be ruled out the detrimental effect of weak ferromagnetic component to the superconductivity in $Y_{1-x}Tb_xNi_2B_2C$.

## V. CONCLUSION

Full series of $Y_{1-x}Tb_xNi_2B_2C$ crystals represents variety of magnetisms and superconductivities, which were seen in

$TbNi_2B_2C$ and $YNi_2B_2C$ and the interplay between them. The superconductivity, AF-ordered state and weak-ferromagnetic state are observed clearly depending upon the Y/Tb concentration ratio. The three transition temperatures, $T_c$, $T_N$, and $T_{WF}$, are all scaled well with de Gennes factor, indicating that the three phenomena are closely correlated. Because there is an overlapping region in which sudden quench of superconductivity accompanies the emergence of the magnetic states, the superconducting pair breaking seems to be more complicated than the AG exchange interaction at $x \approx 0.4$. Not only exchange interaction from AG theory but also interaction with magnetism of AF state and weak-ferromagnetic component should be considered altogether for the detailed model for the pair-breaking in $Y_{1-x}Tb_xNi_2B_2C$.


[1] R. Nagarajan, C. Mazumdar, Z. Hossain, S.K. Dhar, K.V. Gopalakrishnan, L.C. Gupta, C. Godart, B.D. Padalia, and R. Vijayaraghavan, Phys. Rev. Lett. **72**, 724 (1994).

[2] R.J. Cava, H. Tagaki, H.W. Zandbergen, J.J. Krajewski, W.F. Peck, Jr., T. Siegrist, B. Batlogg, R.B. van Dover, R.J. Felder, K. Mizuhashi, J.O. Lee, H. Eisaki, and S. Uchida, Nature (London) **367**, 252 (1994).

[3] H. Eisaki, H. Tagaki, R.J. Cava, B. Batlogg, J.J. Krajewski, W.F. Peck, Jr., K. Mizuhashi, J.O. Lee, and S. Uchida, Phys. Rev. B **50**, 647 (1994).

[4] T. Sigrist, H.W. Zandbergen, R.J. Cava, J.J. Krajewski, and W.F. Peck, Jr., Nature (London) **367**, 254 (1994).

[5] Warren E. Pickett and David J. Singh, Phys. Rev. Lett. **72**, 274 (1994).

[6] L.F. Mattheiss, Phys. Rev. B **49**, 13 279 (1994).

[7] C.V. Tomy, L.A. Afalfiz, M.R. Lees, J.M. Martin, and D. Mck. Paul, Phys. Rev. B **53**, 307 (1996).

[8] B.K. Cho, P.C. Canfield, and D.C. Johnston, Phys. Rev. B **53**, 8499 (1996).

[9] P. Dervenagas, J. Zarestky, C. Stassis, A.I. Goldman, P.C. Canfield, and B.K. Cho, Phys. Rev. B **53**, 8506 (1996).

[10] D.R. Sanchez, M.A.C. de Melo, M.B. Fontes, S.L. Bud'ko, E. Baggio-Saitovitch, M. Hillberg, W. Wagener, H.-H. Klau, G.H. Walf, and F.J. Litterst, Phys. Rev. B **57**, 10 268 (1998).

[11] J.W. Lynn, S. Skanthakumar, Q. Huang, S.K. Sinha, Z. Hossain, L.C. Gupta, R. Nagarajan, and C. Godart, Phys. Rev. B **55**, 6584 (1997).

[12] B.K. Cho, P.C. Canfield, and D.C. Johnston, Phys. Rev. B **52**, R3 844 (1995).

[13] B.K. Cho, P.C. Canfield, and D.C. Johnston, Phys. Rev. Lett. **77**, 163 (1996).

[14] T.E. Grigereit, J.W. Lynn, Q. Huang, A. Santoro, R.J. Cava, J.J. Krajewski, and W.F. Peck, Jr., Phys. Rev. Lett. **73**, 2756 (1994).

[15] Q. Huang, A. Santoro, T.E. Grigereit, J.W. Lynn, R.J. Cava, J.J. Krajewski, and W.F. Peck, Jr., Phys. Rev. B **51**, 3701 (1995).

[16] P. Dervenagas, J. Zarestky, C. Stasiss, A.I. Goldman, P.C. Canfield, and B.K. Cho, Physica B **212**, 1 (1995).

[17] Hyeonjin Doh, Manfred Sigrist, B.K. Cho, and Sung-Ik Lee, Phys. Rev. Lett. **83**, 5350 (1999).

[18] B.K. Cho, P.C. Canfield, L.L. Miller, D.C. Johnston, W.P. Beyermann, and A. Yatskar, Phys. Rev. B **52**, 3684 (1995).

[19] B.K. Cho, B.N. Harmon, D.C. Johnston, and P.C. Canfield, Phys. Rev. B **53**, 2217 (1996).

[20] P.C. Canfield, S.L. Bud'ko, B.K. Cho, A. Lacerda, D. Farrell, E. Johnston-Halperin, V.A. Kalatsky, and V.L. Pokrovsky, Phys. Rev. B **55**, 1 (1997).

[21] H. Bitterlich, W. Loser, G. Behr, K. Nenkov, G. Fuchs, A. Belger, and L. Schultz, Physica C **308**, 243 (1998).

[22] Y.L. Wang, Phys. Lett. **35A**, 383 (1971); Pierre Boutron, Phys. Rev. B **7**, 3226 (1973).

[23] Z.Q. Peng, K. Krug, and K. Winzer, Physica C **317-318**, 441 (1999).